

Article

The Law of Liquid–Solid Carrying in the Wellbore of Natural Gas Hydrate Gas Well under the Condition of Foam Drainage Gas Recovery

Haitao Li ^{1,2,*}, Na Wei ¹, Haiyu Hu ¹, Zhaolong Ge ², Lin Jiang ¹, Fengjun Liu ³, Xiaoran Wang ¹, Chao Zhang ¹, Hanming Xu ¹, Jun Pei ¹ and Bjørn Kvamme ¹

¹ State Key Laboratory of Oil and Gas Reservoir Geology and Exploitation, Southwest Petroleum University, Xindu Road No.8, Chengdu 610500, China

² State Key Laboratory of Coal Mine Disaster Dynamics and Control, Chongqing University, Shazheng Road No.174, Chongqing 400044, China

³ Chengdu Advanced Metal Material Industrial Technology Research Institute Co., Ltd., Huajin Road No.738, Chengdu 610500, China

* Correspondence: 201799010071@swpu.edu.cn

Abstract: During the trial production of marine gas hydrate in the former Soviet Union, Canada, North Slope of Alaska, South Sea Trough of Japan and Shenhu Sea of South China Sea, the problem of sand and water production cannot be avoided. The problems of sand production and water production in the process of natural gas hydrate depressurization exploitation have seriously restricted the exploitation efficiency and production of natural gas hydrate. The problems of sand production and water production are some of the main factors that prevent natural gas hydrate being commercially exploited. Therefore, it is urgent to carry out useful, relevant and cutting-edge research on the efficient drainage of sand and water from the wellbore in the process of natural gas hydrate mining. This paper innovatively proposes liquid-carrying and solid-carrying technology under foam circulation purging to address the existing problems of sand removal and drainage technology in hydrate mining. At present, no scholar has used this technology to solve the problem of sand removal and drainage in hydrate mining. Therefore, the research on efficient drainage is imperative. In this paper, We mainly studied the liquid-carrying and solid-carrying of vertical wellbore under the condition of foam cycle purging. We have revealed the relevant the liquid-carrying law and solid-carrying law through the above research.

Keywords: natural gas hydrate (NGH); foam liquid; continuous drainage and recovery; liquid-carrying law; law of carrying and fixing



Citation: Li, H.; Wei, N.; Hu, H.; Ge, Z.; Jiang, L.; Liu, F.; Wang, X.; Zhang, C.; Xu, H.; Pei, J.; et al. The Law of Liquid–Solid Carrying in the Wellbore of Natural Gas Hydrate Gas Well under the Condition of Foam Drainage Gas Recovery. *Energies* **2023**, *16*, 2414. <https://doi.org/10.3390/en16052414>

Academic Editor: Dmitry Eskin

Received: 20 December 2022

Revised: 5 February 2023

Accepted: 21 February 2023

Published: 2 March 2023



Copyright: © 2023 by the authors. Licensee MDPI, Basel, Switzerland. This article is an open access article distributed under the terms and conditions of the Creative Commons Attribution (CC BY) license (<https://creativecommons.org/licenses/by/4.0/>).

1. Introduction

With the continuous progress and development of society, the reserves of traditional fossil fuels have been greatly reduced and will bring a series of environmental problems. It is imperative to find safe and reliable clean energy. NGH, also known as “combustible ice”, is a cage-like crystalline compound formed by methane, water and other hydrocarbon gases under low temperature and high pressure. Under standard conditions, 1 m³ NGH can be decomposed into 0.8 m³ water and 164 m³ methane gas, and it has the characteristics of high gas storage density and high combustion calorific value [1–3]. As an important replacement energy, natural gas hydrate resources in the South China Sea alone reach 85 × 10¹² m³. The non-diagenetic natural gas hydrate accounts for more than 76.5%, 1.56 times that of the total known amounts of natural gas and 2.1 times that of the national conventional natural gas reserves. Natural gas hydrate is the replacement energy with the greatest exploitation potential after shale gas, coal-bed methane and tight gas. Natural gas hydrate is also an undeveloped unconventional natural gas resource with the greatest resource potential.

Therefore, it has become the commanding point of future energy strategy and the frontier of scientific and technological innovation for all countries in the world [2,4]. At present, the marine gas hydrate samples obtained worldwide are generally characterized by shallow burial depth and weak cementation [2,5,6]. In the process of gas hydrate depressurization, due to the change of pipeline pressure and temperature, the hydrate undergoes phase transformation and decomposition, resulting in the migration and precipitation of gas and water, which leads to serious problems of sand production and water production, which has become an important problem restricting the safe and efficient development of natural gas hydrate [7–11]. During the trial production of marine gas hydrate in the former Soviet Union, Canada, North Slope of Alaska, South Sea Trough of Japan and Shenhu Sea of South China Sea, the problem of sand and water production cannot be avoided, and the output has not reached a commercial scale [12,13]. Therefore, it is imperative to study efficient continuous drainage and production. Foam drainage and gas recovery (FDGR) technology is the injection of a surfactant (foaming agent) that can be bubbled with water into the bottom of the well. After the contact between the bottom hole water and the foaming agent, a large amount of low-density aqueous foam is produced under the stirring action of natural air flow, and then carried from the bottom of the well to the ground with the air flow to achieve the purpose of discharging the fluid in the wellbore [14–16].

Many scholars in academic circles have carried out much research on foam drainage of conventional oil and gas exploitation. Xiong Ying and others simulated the foam drainage process of high-temperature gas wells more realistically. The dynamic performance of foam at 150 °C was evaluated [17]. A.T. van Nimwegen and others carried out a gas–liquid two-phase pipe flow experiment. Photos of foam slug flow were taken with a high-speed camera in the experiment, and the flow pattern characteristics of foam flow were described [18]. Huang Bin et al. studied the mechanism of liquid retention in the wellbore using numerical simulation and laboratory experiments, and analyzed the retention effect of relocators with different structures on reflux fluid [19]. Huang Bin and others established the coupling model and numerical solution method of gas and foam flow in the wellbore [20]. A. J. Chamkha carried out research on the boundary layer theory of particle suspension and particle viscosity effect. The particle–fluid viscosity ratio and viscosity–temperature relationship are very helpful for this paper in wellbore pressure calculation and temperature calculation. The wall heat transfer coefficient, skin-friction coefficients and displacement thickness for both the particle and fluid phases are of great help in the calculation of the volume fraction of the gas–liquid–solid phase and wellbore temperature in this paper. The particulate viscous and diffusion effects are very helpful in this paper in the calculation of wellbore pressure and the volume fraction of the gas–liquid–solid phases [21–24]. Zeinab Derikvand et al. experimented with four types of water foam by changing the viscosity of the water phase using a low-cost polymer (i.e., carboxymethyl cellulose gum; CMC) to determine the optimum condition for a transparent porous fabric to maximize the performance of a foam injection [25]. On the basis of analyzing the characteristics and applicable conditions of gas extraction, Du Zehong proposed the technique of gas extraction by small diameter tubing in horizontal wells without killing the well. According to the theoretical analysis, the experiment is feasible, and the experimental results obtained by the field experiment are remarkable [26]. Li Rui et al. selected bovine serum albumin (BSA) as the model protein to study the effect of increasing bubble size on foam-induced protein aggregation [27]. Wen Yiping et al. prepared a natural gas foam system using alkyl polyglycoside (APG) as a foaming agent and natural gas as the gas phase. The influence of concentration, metal cation valence and alkyl chain length, and the foam stability influenced by polymer types were studied [28]. Wang Hongbing et al. constructed a range of fatty alcohol polyoxyethylene ether sulfate (AES) foam models at different lifting stages from well to ground by the molecular dynamics simulation method. The foam stability influenced by temperature and pressure was studied [29]. Fan Xinke et al. studied and analyzed the performance of the foam produced by the composite solution formed by the mixture of bio-based lignin nanoparticles (LNPs) and surfactants [30]. Lai Nanjun

studied the coarsening behavior of APG foam and the variation rule of different gasses in the drainage process, and the molecular behavior and interaction of APG in different gas phases were analyzed by molecular simulation [31].

There are some differences between the foam circulation purging liquid-carrying and solid-carrying process innovatively proposed in this paper and the conventional foam drainage and production process. The conventional foam drainage and production process usually uses the produced gas flow to stir the foam drainage agent fully and the formation water foams at the bottom of the hole. Then, under the action of differential pressure, the produced gas and foam carrying water and sand are discharged along the tubing. However, in the foam drainage and production process of hydrate production engineering, the rate of hydrate depressurization and decomposition into natural gas in the reservoir is relatively slow. The natural gas decomposed from the hydrate reservoir enters the wellbore slowly, and the gas flow into the wellbore is small and slow. It fails to meet the requirements for efficient treatment of bottom hole fluid accumulation and sand production. Therefore, the foam drainage and production process applied to hydrate production requires putting another pipeline into the original oil pipe, as shown in Figure 1. This pipeline is used to inject the foam drainage agent and gas into the bottom of the well. The purpose of gas injection is to increase the gas flow and fully form foam to improve the efficiency of liquid- and solid-carrying. The injected gas and produced gas fully agitate the foam drainage agent, and the formation water foams at the bottom of the hole to form foam. The formed foam carries the sand and water produced at the bottom of the well and circulates out along the annulus between the injection pipeline and the tubing. Finally, the sand and water produced at the bottom of the well are discharged from the wellbore to achieve the purpose of clear sediment and bottom-hole liquid accumulation, making the exploitation of natural gas hydrate feasible in the long term. FDGR is one of the most widely used drainage and production technologies due to its fast performance and low cost [32]. Despite the rapid development and promising application prospect of FDGR technology, there is no precedent for its application in hydrate reservoir exploitation. There is little research on the law of liquid–solid carrying of foam fluid in wellbore annulus, which is far from the engineering application. Therefore, it is urgent to study the continuous production efficiency of wellbore multiphase flow under the condition of foam drainage and recovery.

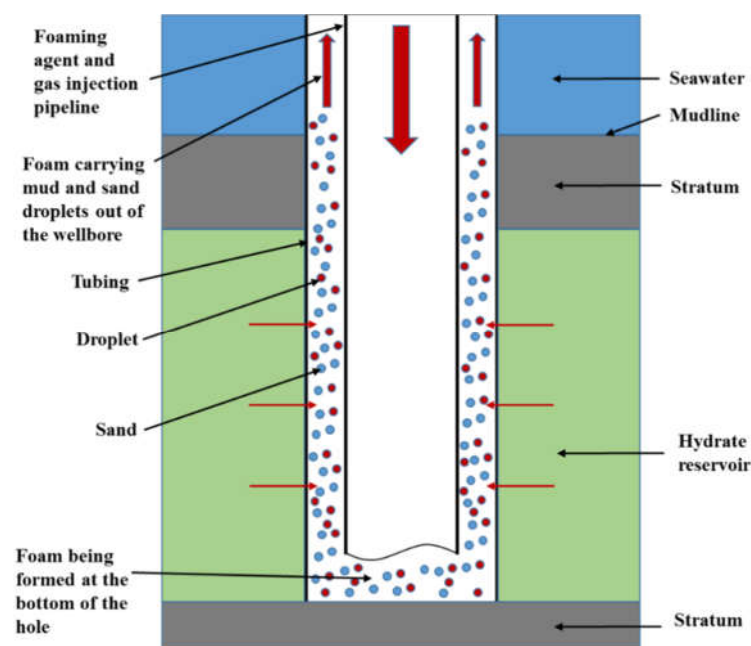


Figure 1. Foam drainage and gas recovery technology schematic diagram.

2. Mathematical Model of Multiphase Flow in Continuous Drainage and Production Wellbore

2.1. Continuity Equation

Considering the influence of hydrate phase transition, the mathematical theoretical model of multiphase flow in continuous drainage and production wellbore is obtained:

$$\frac{\partial}{\partial t}(A\rho_g\alpha_g) + \frac{\partial}{\partial z}(A\rho_g\alpha_g v_g) = q_g \quad (1)$$

$$\frac{\partial}{\partial t}(A\rho_l\alpha_l) + \frac{\partial}{\partial z}(A\rho_l\alpha_l v_l) = q_l \quad (2)$$

where q_l is the mass change of the liquid phase in wellbore multiphase flow caused by hydrate phase transition, kg/m^3 ; q_g is the mass change of the gas phase in wellbore multiphase flow caused by hydrate phase transition, kg/m^3 ; ρ_g is the liquid phase density, kg/m^3 ; v_l is the liquid phase velocity, m/s ; v_g is the gas phase velocity, m/s ; α_l is liquid-holdup, liquid percentage, dimensionless; and α_g is gas-holdup, gas phase percentage, dimensionless.

2.2. Equation of Motion

Equation of motion of multiphase flow in continuous wellbore is

$$\begin{aligned} \frac{\partial}{\partial t}(\rho_g\alpha_g v_g + \rho_l\alpha_l v_l + \rho_s\alpha_s v_s) + \frac{\partial}{\partial z}(p + \rho_g\alpha_g v_g^2 + \rho_l\alpha_l v_l^2 + \rho_s\alpha_s v_s^2) \\ + (\rho_g\alpha_g + \rho_l\alpha_l + \rho_s\alpha_s)g \sin \theta + \frac{\lambda\rho_m v_m^2}{2(D_{ci} - D_{po})} = 0 \end{aligned} \quad (3)$$

2.3. Wellbore Pressure Field Model

Pressure gradient equation is

$$\frac{dp}{dz} = -(\rho g \sin \theta + f \frac{\rho v^2}{2D} + \rho v \frac{dv}{dz}) \quad (4)$$

where the total pressure drop gradient can be expressed as the sum of the three components by the following formula, namely gravity pressure drop, frictional pressure drop and kinetic energy pressure drop gradient (expressed by subscripts G , F and A , respectively).

$$\frac{dp}{dz} = \left(\frac{dp}{dz}\right)_G + \left(\frac{dp}{dz}\right)_F + \left(\frac{dp}{dz}\right)_A \quad (5)$$

where θ is the pipe inclination, $^\circ$, $\theta = 90^\circ$ in the vertical well; g is the acceleration of gravity, m/s^2 ; p is the pressure, Pa ; and f is the frictional drag coefficient, dimensionless. In the formula, coordinate z is positively taken as the direction of fluid flow, so the total pressure gradient $\frac{dp}{dz}$ is negative, indicating that the pressure decreases along the direction of flow.

2.4. Wellbore Temperature Field Model

The system of mixed fluid, coiled tubing, tubing, surface casing, cement ring, formation and seawater in the wellbore continuously exchanges heat, and the temperature in the coiled tubing is constantly changing, as shown in Figure 2.

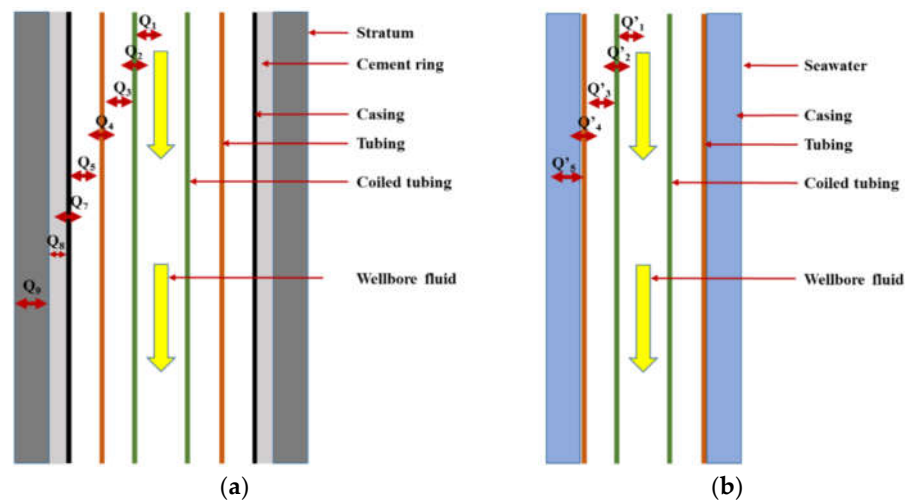


Figure 2. Schematic diagram of wellbore heat transfer. (a) Below the mud line. (b) Above the mud line.

2.4.1. Below the Mud Line

The convective heat transfer process under the mud line is the convection heat transfer between the coiled tubing wall and the gas–liquid mixed fluid in the wellbore, the heat conduction between the inner and outer surface of the coiled tubing, the heat conduction between the coiled tubing outer surface and coiled tubing, the convective heat transfer in the tubing annulus, the heat conduction between the inner surface and outer surface of the tubing, the convective heat transfer between the outer surface of the tubing and the casing annulus, the heat conduction between the inner surface and outer surface of the casing, the heat conduction between the inner surface and outer surface of the cement ring, and the heat conduction between the cement ring outer surface and stratum. The calculation method of each parameter is as follows:

The convective heat transfer between the gas–liquid mixed fluid in the wellbore and coiled tubing wall is

$$Q_1 = \pi D_{oi} v_m h_1 (T_g - T_{oi}) \tag{6}$$

where D_{oi} is the coiled tubing inner diameter (m); v_m is the mixed fluid flow velocity in the coiled tubing, (m/s); T_{oi} is the internal wall temperature of the coiled tubing (K); T_g is the temperature of the mixed fluid in the coiled tubing (K); and h_1 is the convective heat transfer coefficient between the coiled tubing mixed fluid and the coiled tubing inner surface, (W/m·K).

The heat conduction between the inner and outer surface of the coiled tubing is

$$Q_2 = \frac{T_{oi} - T_{oo}}{\frac{1}{2\pi\lambda_1 v_m} \ln \frac{D_{oo}}{D_{oi}}} \tag{7}$$

where T_{oo} is the outer surface temperature of the coiled tubing (K); D_{oo} is the coiled tubing outer diameter (m); D_{oi} is the coiled tubing inner diameter (m); and λ_1 is the coiled tubing thermal conductivity (W/m·K).

The heat conduction between the coiled tubing outer surface and coiled tubing, and the convective heat transfer in the tubing annulus are

$$Q_3 = \pi D_{oc} v_m h_2 (T_{oo} - T_{di}) \tag{8}$$

where D_{oc} is the equivalent diameter of the coiled tubing and tubing annulus (m); h_2 is the natural convection heat transfer coefficient of the coiled tubing and tubing ring (W/m·K); and T_{di} is the temperature of the inner surface of the tubing (K).

The heat conduction between the inner surface and outer surface of the tubing is

$$Q_4 = \frac{T_{di} - T_{do}}{\frac{1}{2\pi\lambda_2 v_m} \ln \frac{D_{do}}{D_{di}}} \quad (9)$$

where T_{do} is the outer surface temperature of the tubing (K); D_{do} is the tubing outer diameter (m); D_{di} is the tubing inner diameter (m); and λ_2 is the thermal conductivity coefficient of the tubing, and is numerically equivalent to the thermal conductivity of the coiled tubing λ_1 (W/m·K).

The convective heat transfer between the outer surface of the tubing and casing annulus is

$$Q_5 = \pi D_{dc} v_m h_3 (T_{oo} - T_{di}) \quad (10)$$

where D_{dc} is the equivalent diameter between the outer surface of the tubing and the casing annulus (m); h_3 is the natural convection heat transfer coefficient between the outer surface of the tubing and casing annulus gas, and is numerically equal to the natural convection heat transfer coefficient h_2 of the coiled tubing and the tubing annulus gas (W/m·K); and T_{di} is the temperature of the inner surface of the tubing (K).

The heat conduction between the inner surface and outer surface of the casing is

$$Q_6 = \frac{T_{ci} - T_{co}}{\frac{1}{2\pi\lambda_3 v_m} \ln \frac{D_{co}}{D_{ci}}} \quad (11)$$

where T_{co} is the casing outer surface temperature (K); D_{co} represents the casing outer diameter (m); D_{ci} is the casing inner diameter (m); and λ_3 is the thermal conductivity of the casing and is numerically equivalent to the coiled tubing thermal conductivity λ_1 (W/m·K).

The heat conduction between the inner surface and outer surface of the cement ring is

$$Q_7 = \frac{T_{si} - T_{so}}{\frac{1}{2\pi\lambda_4 v_m} \ln \frac{D_{so}}{D_{si}}} \quad (12)$$

where T_{so} represents the outer surface temperature of the cement ring (K); T_{si} is the temperature of the inner surface of the cement ring (K); D_{so} represents the outer diameter of the cement ring (m); D_{si} represents the inner diameter of the cement ring, and is numerically equal to the casing outer diameter D_{co} (m); and λ_4 is the thermal conductivity of the cement ring (W/m·K).

The heat conduction between the cement ring outer surface and stratum is

$$Q_8 = \frac{T_{so} - T_f}{\frac{1}{2\pi\lambda_5 v_m} \ln \frac{D_f}{D_{so}}} \quad (13)$$

where T_f is the original stratum temperature (K); λ_5 is the thermal conductivity of the stratum (W/m·K); and D_f is the stratum diameter in the range of action (m).

According to the constant deformation of convection and heat transfer between the mixed fluid and the wellbore in the coiled tubing, the heat flux between the mixed fluid and the wellbore in the coiled tubing can be expressed as follows:

$$q = \frac{\pi D_{oi} U_1}{Q_m} (T_m - T_{so}) \quad (14)$$

where Q_m is the volume flow rate of mixed fluid in the wellbore (m³/s); and U_1 represents the comprehensive heat transfer coefficient between the wellbore and stratum (W/(m²·K)). In the last formula, U_1 is expressed as

$$U_1 = \frac{1}{\frac{1}{h_1} + \frac{D_{oi} \cdot \ln(\frac{D_{oo}}{D_{oi}})}{2\lambda_1} + \frac{D_{oi}}{D_{oc}h_2} + \frac{D_{oi} \cdot \ln(\frac{D_{de}}{D_{di}})}{2\lambda_2} + \frac{D_{di}}{D_{dc}h_3} + \frac{D_{oi} \cdot \ln(\frac{D_{ce}}{D_{ci}})}{2\lambda_3} + \frac{D_{oi} \cdot \ln(\frac{D_{so}}{D_{si}})}{2\lambda_4} + \frac{D_{oi} \cdot \ln(\frac{D_f}{D_{so}})}{2\lambda_5}} \tag{15}$$

According to Ramney [33], the heat flow from the distal stratum to the wellbore is

$$q = \frac{2\pi k_f}{Q_m T_D} (T_{ei} - T_{so}) \tag{16}$$

where k_f is the thermal conductivity of the formation (W/m·K); Q_m is the mass flow of mixed fluid in the wellbore (kg/s); T_{ei} is the original stratum temperature (K); T_w is the wellbore temperature (K); and T_D is a dimensionless temperature.

Because the heat transferred from the wellbore to the formation is equal to the heat transferred from the wellbore fluid to the wellbore, the heat transferred from the stratum to the wellbore fluid can be obtained after simplification:

$$q = \frac{c_m}{A} (T_{ei} - T_m) dz \tag{17}$$

$$A = \frac{c_m Q_m (k_f + \frac{D_{oi} U_1 T_D}{2})}{\pi D_{oi} U_1 k_f} \tag{18}$$

where c_m is the specific heat capacity of the mixed fluid in the wellbore (J/kg·K).

2.4.2. Above Mud Line

Similarly, the heat transfer process above the mud line from inside to outside is convective heat transfer between the gas–liquid mixed fluid in the coiled tubing and the inner surface of the coiled tubing, the heat conductivity between the inner and outer surface of the coiled tubing, the convective heat transfer of the coiled tubing and tubing annulus, the heat conduction between the inner surface and outer surface of the tubing and the convective heat transfer between the tubing and seawater.

The calculation method of each parameter is as follows:

The convection heat transfer between the gas–liquid mixed fluid in the coiled tubing and the inner surface of coiled tubing is

$$Q'_1 = \pi D_{oi} v_m h_1 (T_m - T_{oi}) \tag{19}$$

where D_{oi} is the coiled tubing inner diameter (m); T_{oi} is the internal wall temperature of the coiled tubing (K); T_m is the temperature of the mixed fluid in the coiled tubing (K); and h_1 is the convective heat transfer coefficient between the coiled tubing mixed fluid and the coiled tubing inner surface, (W/m·K).

The heat conduction between the inner and outer surface of the coiled tubing and well section below the mud line identically is

$$Q'_2 = \frac{T_{oi} - T_{oo}}{\frac{1}{2\pi\lambda_1 v_m} \ln \frac{D_{oo}}{D_{oi}}} \tag{20}$$

where T_{oo} is the outer surface temperature of the coiled tubing (K); D_{oo} is the coiled tubing outer diameter (m); D_{oi} is the coiled tubing inner diameter (m); and λ_1 is the coiled tubing thermal conductivity (W/m·K).

The convective heat transfer in the coiled tubing and tubing annulus are

$$Q'_3 = \pi D_{omr} v_m h'_2 (T_{oo} - T_{mri}) \tag{21}$$

where D_{omr} is the equivalent diameter of the coiled tubing and tubing annulus (m); T_{oo} is the outer surface temperature of the coiled tubing (K); T_{mri} is the temperature of the inner

surface of the tubing (K); and h'_2 is the natural convection heat transfer coefficient of the coiled tubing and tubing ring (W/m·K).

The heat conduction between the inner surface and outer surface of tubing is

$$Q'_4 = \frac{T_{mri} - T_{mro}}{\frac{1}{2\pi\lambda'_2 v_m} \ln \frac{D_{mro}}{D_{mri}}} \quad (22)$$

where T_{mro} is the outer surface temperature of the tubing (K); D_{mro} is the tubing outer diameter (m); D_{mri} is the tubing inner diameter (m); and λ'_2 is the thermal conductivity coefficient of the tubing (W/m·K).

The convective heat transfer between the tubing and seawater is

$$Q'_5 = \pi D_{mro} v_m h'_3 (T_{mro} - T_{sea}) \quad (23)$$

where h'_3 is the convective heat transfer coefficient between the outer surface of the tubing and the seawater; and T_{sea} is the seawater temperature.

3. Research on the Law of Liquid–Solid Carrying in Foam Cycle Purge

3.1. Research on Liquid-Carrying Law of Foam Cycle Purging Wellbore

In the study of the technical scheme of the foam cycle purge and liquid-carrying law, the numerical simulation is carried out based on the gas hydrate reservoir in the South China Sea. The basic parameters are as follows: well depth 1505 m, water depth 1225 m, rig floor to sea level 27 m, tubing size 177.8 mm, coiled tubing size 88.9 mm, and sea surface temperature 25 °C. The well structure is shown in Table 1.

Table 1. Calculation of well structure using the foam cycle purge technique.

Interval	Bit Size mm	Casing Size mm	Casing Running Interval m	Depth of Cement Return
1	660.4	914.4	0~62	Mud line
2	460	339.7	0~207	Mud line
3	311.2	244.5	0~253	Mud line

Combined with the theoretical model of liquid-carrying in the continuous drainage wellbore, using the foam cycle purge method, under the conditions of gas production of 20,000 m³/d, liquid injection of 0.5 m³/min, sand production of 10 m³/d, foam viscosity of 8 mPa·s and solid particle size of 1 mm, numerical calculation is carried out under the conditions of water production of 5 m³/d, 10 m³/d and 15 m³/d, respectively. The bottom hole pressure, bottom hole temperature, maximum mixture density, minimum liquid-carrying capacity, maximum liquid-carrying capacity, minimum solid-carrying capacity, maximum solid-carrying capacity, minimum phase velocity, minimum velocity of liquid phase and solid phase, minimum gas-holdup, maximum liquid-holdup and maximum solid phase content are obtained under different foam injection quantities.

Taking the water production of 10 m³/d as an example, the wellbore flow behavior under the condition of 60 m³/min foam injection is shown as Figure 3.

The variation rules of parameters under different foam injection quantities are shown in Figure 4.

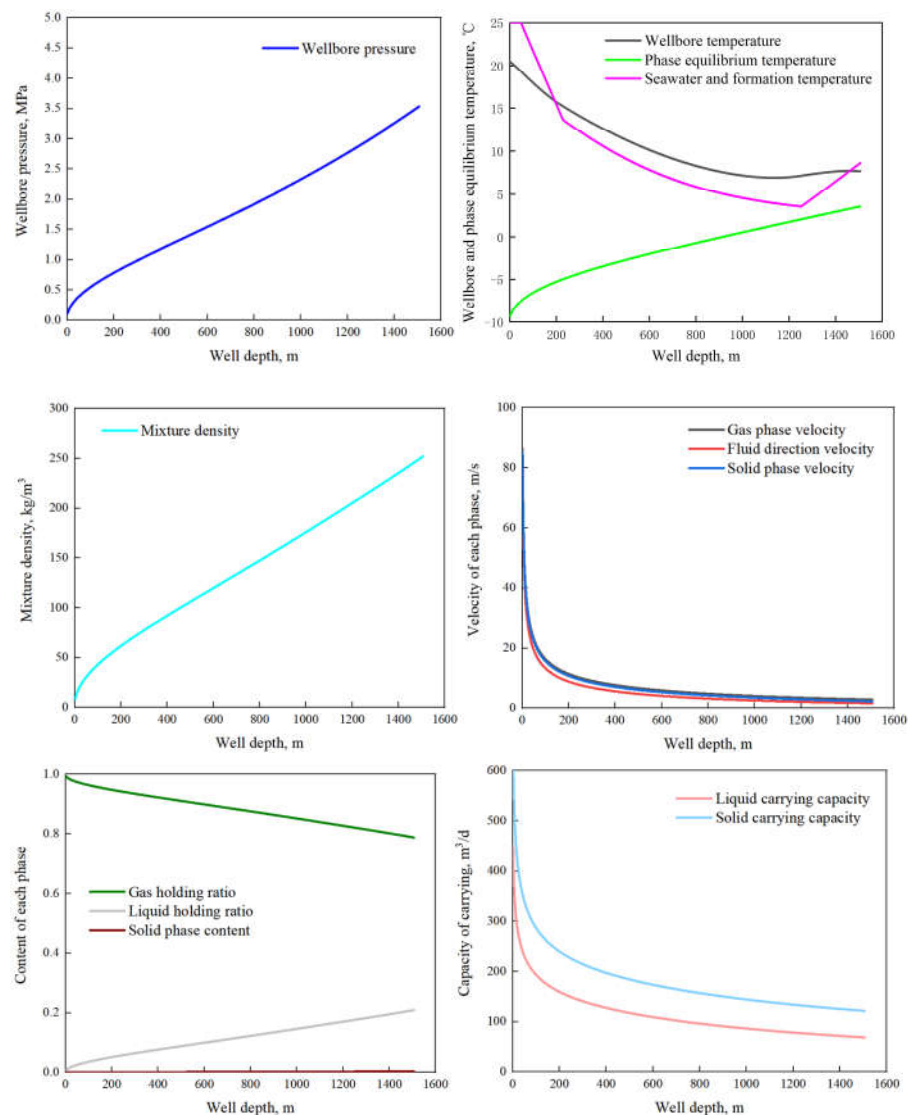


Figure 3. Flow behavior of liquid-carrying wellbore with foam injection volume of $60 \text{ m}^3/\text{min}$.

By comparing any water production and different foam injection quantity conditions, it can be seen that, as the amount of foam injected increases, the bottom hole pressure increases with the influence of mixed density and friction pressure drop, and the increase range is first small and then large; the bottom hole temperature decreases; the capacity of liquid-carrying and solid-carrying increases; the minimum gas phase velocity increases, the gas phase velocity increases and the liquid-carrying capacity increases, so the minimum velocity of the liquid phase increases, the velocity of the gas phase increases and the capacity of solid-carrying increases, so the minimum velocity of the solid phase increases; with the increase of liquid-carrying capacity and solid-carrying capacity, the minimum gas-holdup capacity increases, the maximum liquid-holdup capacity and maximum solid phase content decrease; in the low range, as the volume of foam injection increases, the maximum liquid-holdup rate and the maximum solid phase content have a high change range, while, when the foam injection volume increases to a certain extent, the maximum liquid-holdup rate and the maximum solid phase content have a very low change range. Under this condition, the continuous increase of the foam injection volume will not significantly improve the liquid- and solid-carrying effect.

By comparing the same volume of foam injection and different water production conditions, it can be seen that the liquid-carrying capacity and solid-carrying capacity decrease with the increase of water production; the pressure of the bottom hole increases;

the temperature of the bottom hole increases; the maximum mixture density increases; the minimum gas phase velocity decreases and the liquid-carrying capacity decreases, so the minimum velocity of the liquid phase decreases. As the minimum gas phase velocity decreases, the solid-carrying capacity decreases, so the minimum solid phase velocity decreases; and the minimum gas-holdup rate decreases. As the minimum gas-holdup rate decreases, the capacity of liquid-carrying decreases, so the maximum liquid-holdup rate increases. The minimum gas-holdup rate decreases and the solid-carrying capacity decreases, so the maximum solid phase content increases.

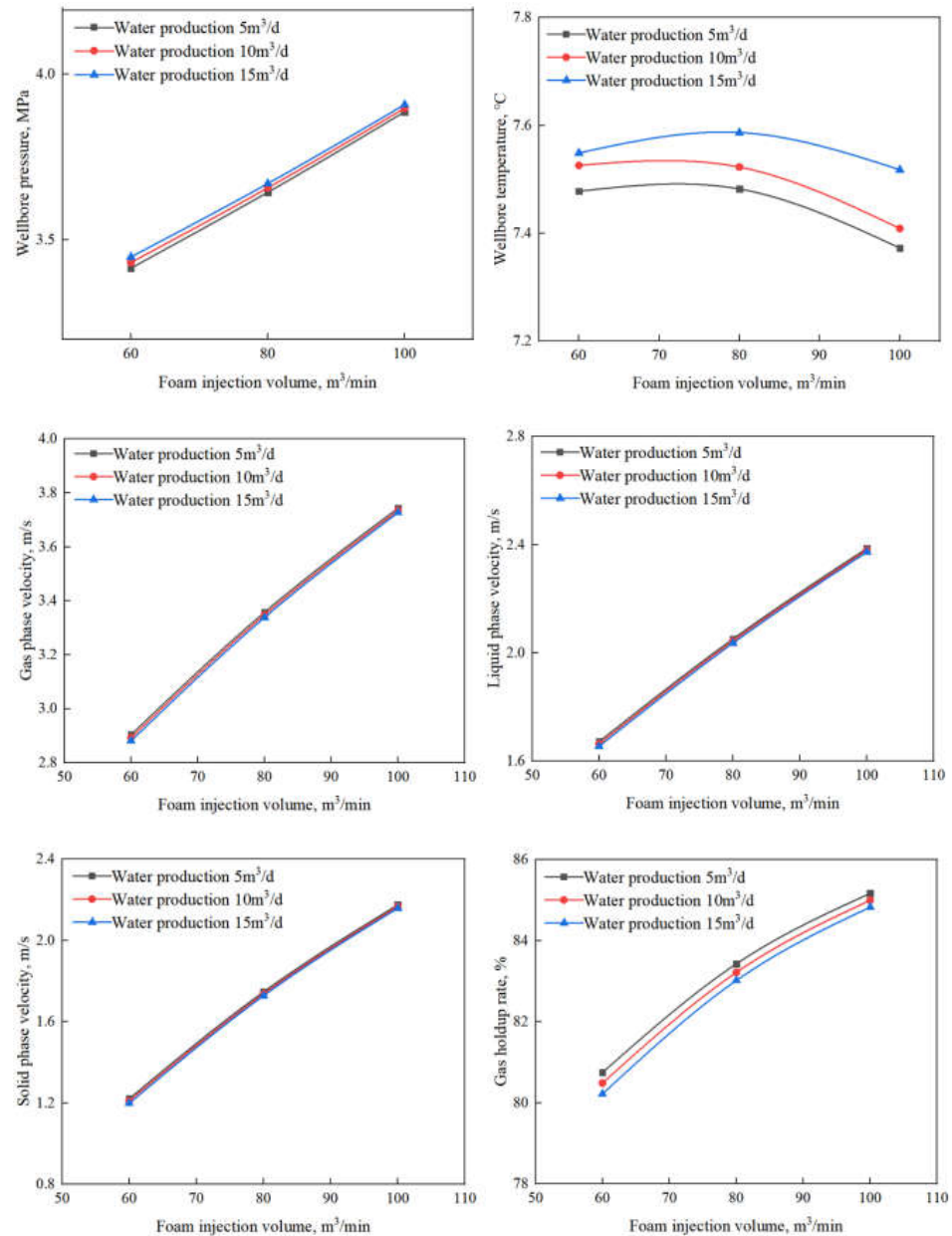


Figure 4. Cont.

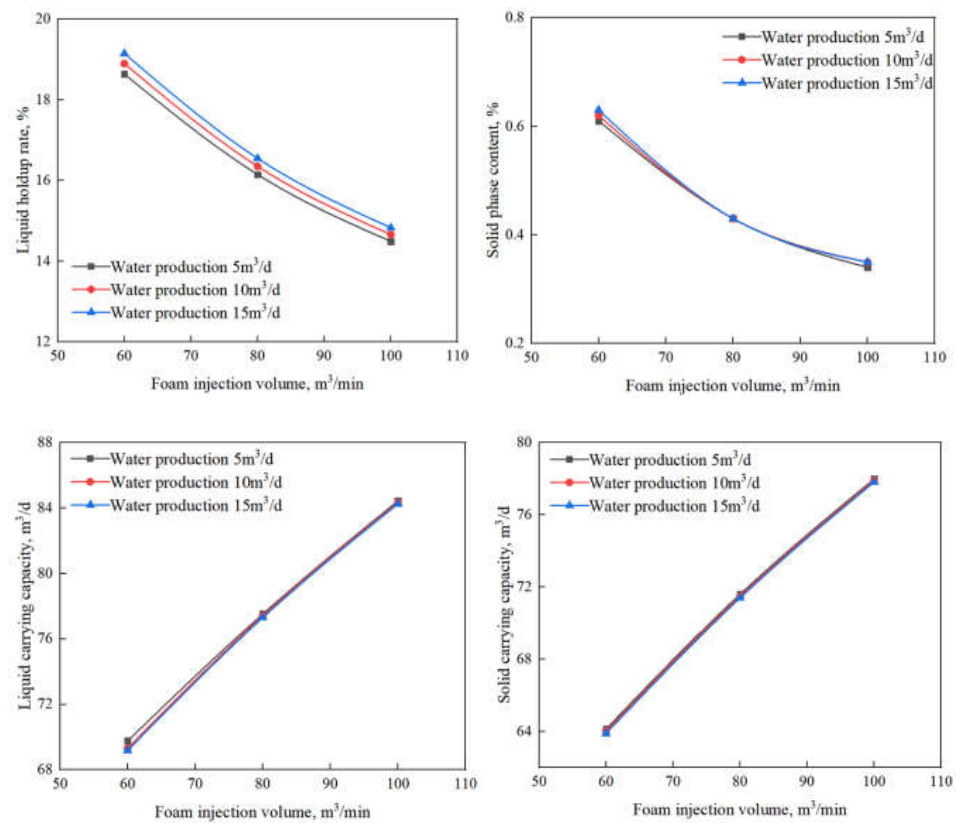


Figure 4. Variation rules of parameters under different foam injection volume at different water production amounts.

3.2. Research on Solid-Carrying Law of Foam Cycle Purging Wellbore

Based on the basic parameters consistent with those used in the research on the law of foam cycle purge and liquid-carrying above, combined with the theoretical model of liquid-carrying in the continuous drainage wellbore, using the foam cycle purge method, under the conditions of gas production of 20,000 m³/d, water production of 10 m³/d, foam viscosity of 8 mPa·s, solid particle size of 1 mm and foam gas–liquid ratio of 120, numerical calculations are carried out under the conditions of sand production of 5 m³/d, 10 m³/d and 15 m³/d, respectively, The bottom hole pressure, bottom hole temperature, maximum mixing density, minimum liquid-carrying capacity, maximum liquid-carrying capacity, minimum solid-carrying capacity, maximum solid-carrying capacity, minimum phase velocity, minimum velocity of liquid phase and solid phase, minimum gas-holdup, maximum liquid-holdup and maximum solid phase content are obtained under different foam injection quantities.

Taking the sand production rate of 10 m³/d as an example, the wellbore flow behavior under the condition of a foam injection rate of 100 m³/min is shown in Figure 5.

The variation rules of parameters of sand production under different foam injection volumes are shown in Figure 6.

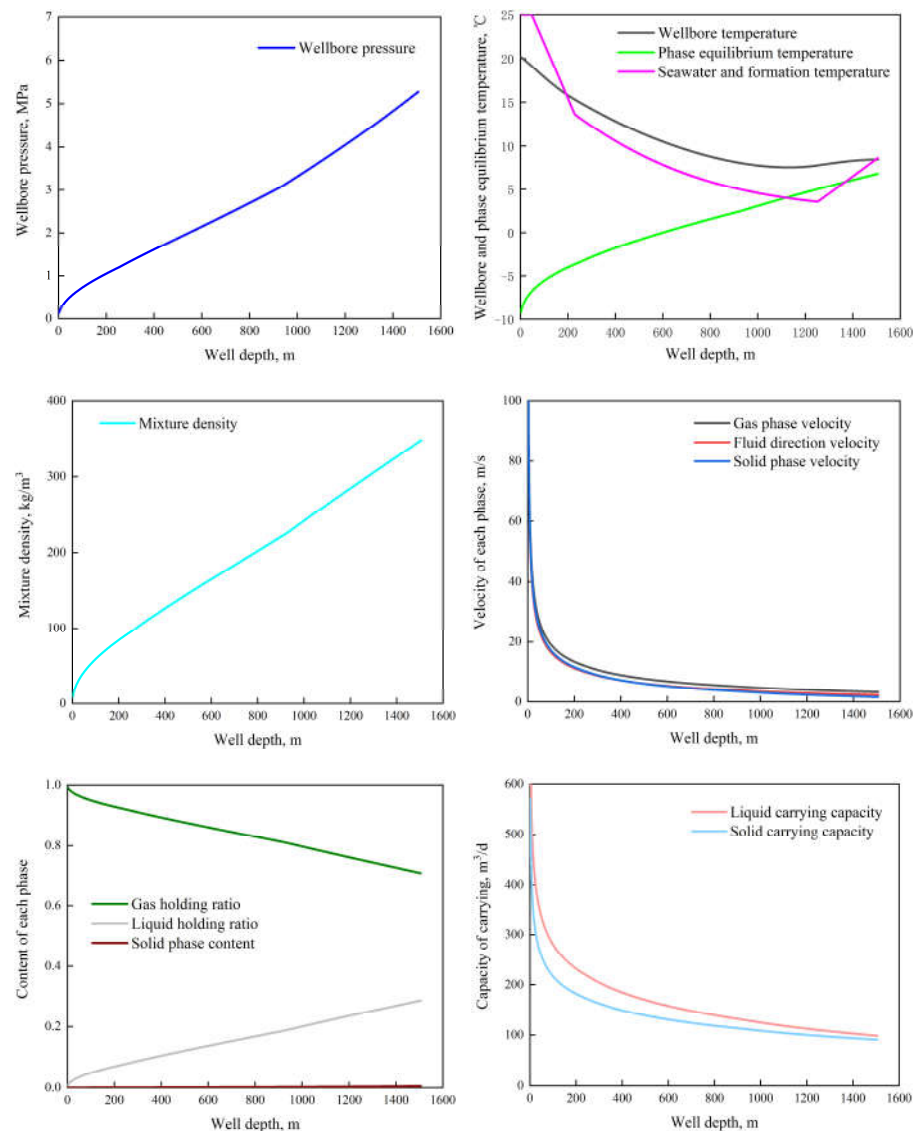


Figure 5. Flow behavior of solid-carrying wellbore with foam injection volume of $60 \text{ m}^3/\text{min}$.

By comparing the sand production of any one and different foam injection quantity conditions, it can be seen that as the amount of foam injected increases, and the liquid-carrying capacity and solid-carrying capacity increase under the influence of mixture density and friction pressure drop; the pressure of the bottom hole increases, and the increase range is first small and then large; the bottom hole temperature decreases; with the increase of the maximum mixing density, the increasing range is first small and then large; the liquid-carrying capacity and solid-carrying capacity increase; the minimum gas phase velocity increases; as the minimum velocity of the gas phase increases, the capacity of liquid-carrying increases, so the minimum velocity of the liquid phase increases. As the minimum velocity of the gas phase increases, the solid-carrying capacity increases, so the minimum velocity of the solid phase increases. The maximum gas-holdup rate decreases; the minimum liquid-holdup increases, so the maximum solid phase content decreases. In the low range, as the volume of foam injection increases, the maximum liquid-holdup rate and the maximum solid phase content have a high change range, while, with the volume of foam injection increasing to a certain extent, the maximum liquid-holdup rate and the maximum solid phase content have a very low change range. Under this condition, the continuous increase of foam injection volume will not significantly improve the liquid- and solid-carrying effect.

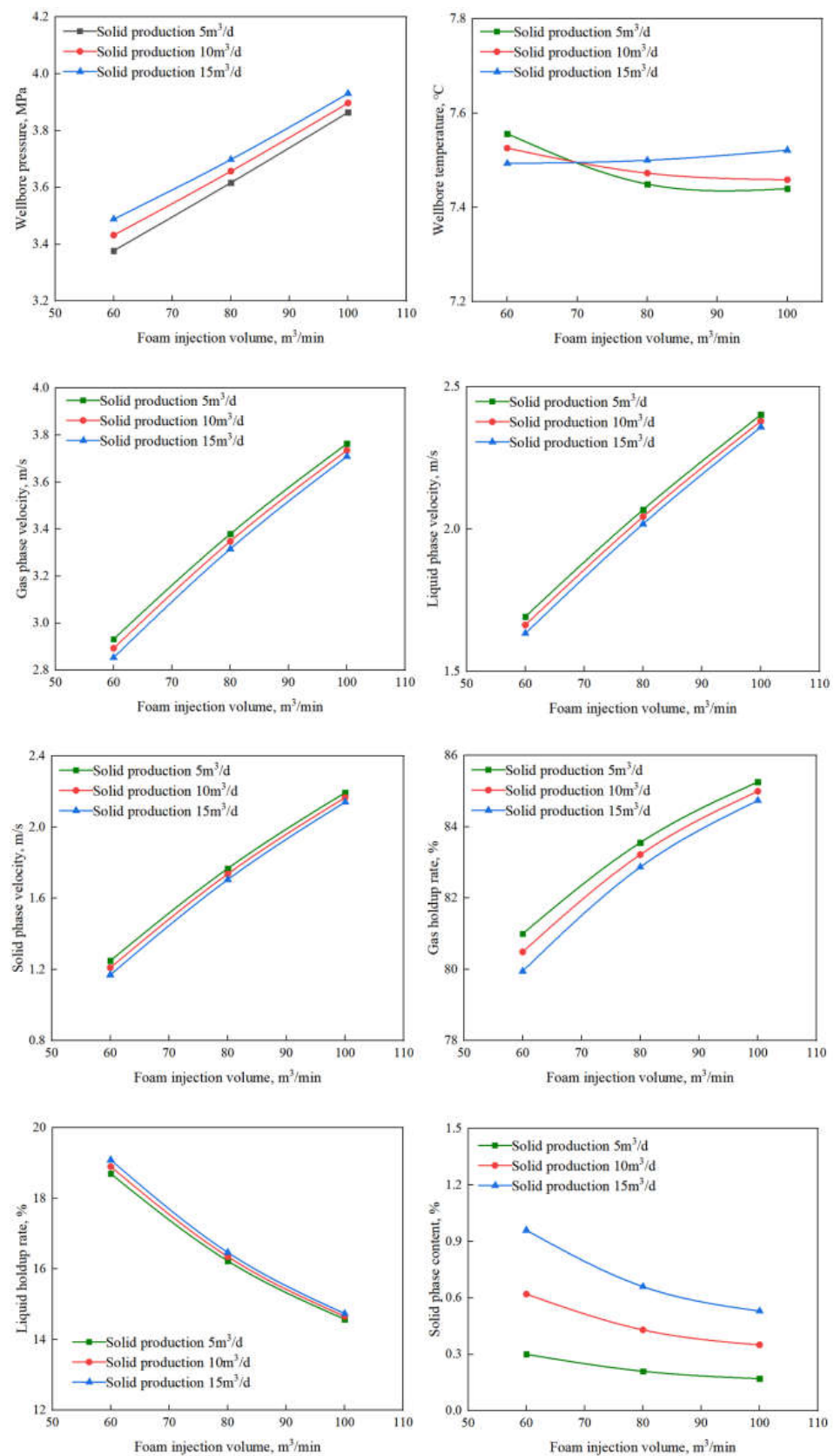


Figure 6. Cont.

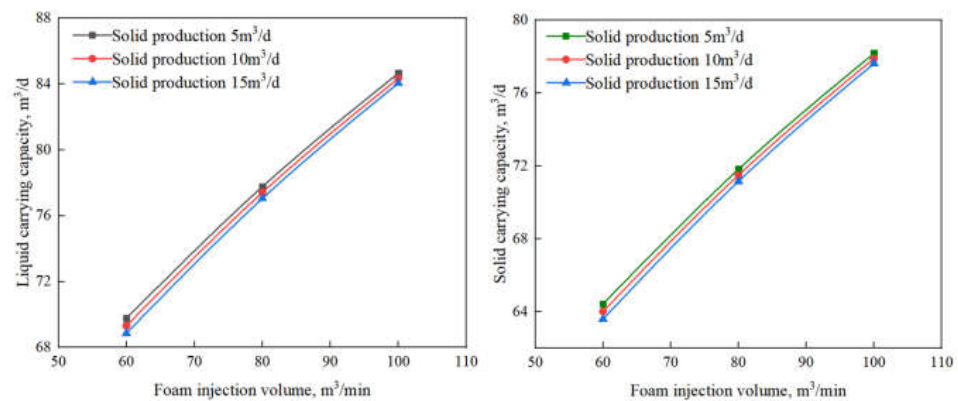


Figure 6. Variation rules of parameters under different foam injection volumes at different solid production values.

By comparing the same amount of foam injection and different sand production conditions, it can be seen that, with the increase of sand production, the liquid-carrying capacity and solid-carrying capacity decrease; the pressure of the bottom hole increases; the bottom hole temperature decreases; the maximum mixing density increases; the minimum gas phase velocity decreases; as the gas phase velocity decreases, the liquid-carrying capacity decreases, so the minimum liquid phase velocity decreases. As the solid-carrying capacity and the velocity of gas phase decreases, so the minimum solid phase velocity decreases. As the minimum gas-holdup decreases, the maximum liquid-holdup increases, and the maximum solid phase content increases.

4. Laboratory Experiment

4.1. Experimental Equipment

The foam drainage and production experimental equipment is mainly composed of vertical pipe transport system, air compressor, gas storage tank, camera and other equipment. The experimental section is a visual plexiglass tube with a height of 15.05 m, inner diameter of 24 mm and outer diameter of 30 mm, as shown in Figure 7; The air compressor is shown in Figure 8; The gas storage tank is shown in Figure 9; The camera has a pixel resolution of 1928 × 1088; The solid particle size is selected as 1 mm, as shown in Figure 10. The UT-4 foaming agent with a mass concentration of 0.5% is selected, as shown in Figure 11.

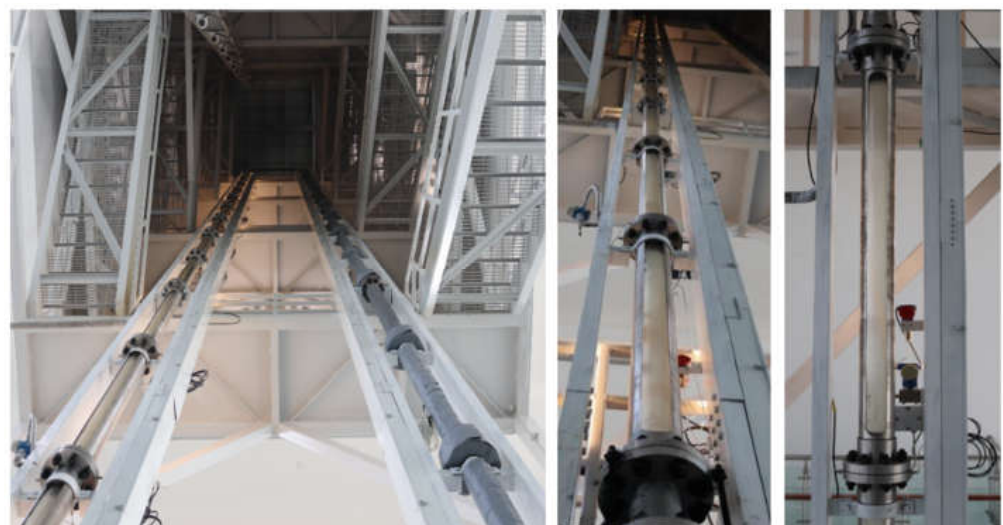


Figure 7. Vertical pipe transport system.



Figure 8. Air compressor.



Figure 9. Gas storage tank.



Figure 10. Solid phase particle.



Figure 11. Foam for experiment.

4.2. Experimental Procedure

The experimental steps are as follows

- (1) Through the sand filling port, add an appropriate amount of foam, water and solid particles to the bottom of the wellbore to simulate the bottom hole sand production and bottom hole fluid accumulation after the exploitation of marine NGH;
- (2) Turn on the power supply, turn on the camera, and start the software to record data;
- (3) Open the air compressor and gradually adjust the air compressor displacement. When solid particles can be carried at the top of the experimental pipe section, namely the wellhead, the gas volume is considered to be the critical flow rate under the experimental conditions. Stabilize the output displacement of the air compressor for 2–5 min, and record the motion state of the solid particles with the camera;
- (4) Increase the displacement and close the air compressor after all solid particles are discharged;
- (5) Add the same amount of solid particles, stabilize the nitrogen injection amount at a certain value, and repeat the experimental steps (2) and (3);
- (6) Save and close the software, turn off the main power supply and high-speed camera, check each valve, clean and tidy the experiment site, and the experiment is over.

4.3. Experimental Phenomena

The experimental phenomenon is shown in Figure 12.



Figure 12. Experimental phenomenon of nitrogen injection of $60 \text{ m}^3/\text{h}$ and particle size of 1 mm.

4.4. Experimental Results and Analysis

According to the experimental data and the theoretical calculation value, the theoretical and experimental comparison curve of wellbore rheological parameters is obtained, and the results are shown in Figure 13.

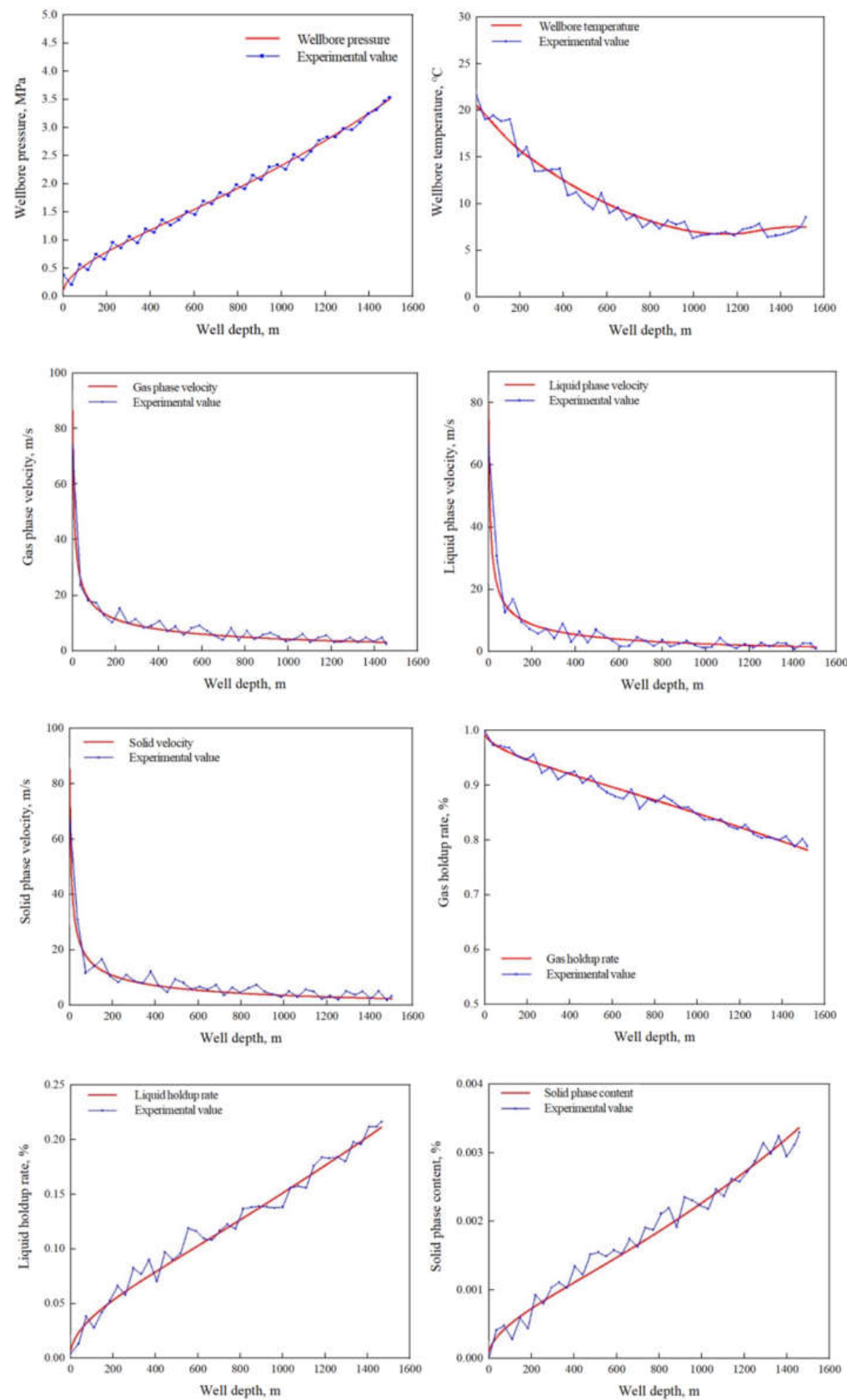


Figure 13. Comparison curve between theoretical and experimental values of wellbore rheological parameters.

As can be seen from the figures, the variation trend of the theoretical values is consistent with that of the experimental values, and the errors are both small, within 10%, which verifies the accuracy of the theoretical model of continuous drainage multiphase flow.

5. Conclusions

In this paper, a multi-phase flow mathematical model of the continuous wellbore is first established. On the basis of MathCAD software, the variation rules of rheological parameters under the conditions of the same aqueous production, different foam injection volumes, the same sand production volume and different foam injection volumes are calculated, and the liquid- and solid-carrying rules of the wellbore under the foam cyclic blowing are obtained.

- (1) Under the same water production condition, the liquid-carrying capacity and solid-carrying capacity are significantly enhanced with the increasing volume of foam injection. However, once the foam injection volume is increased to a certain level, the liquid and solid-carrying effects cannot be significantly improved with the volume of foam injection continuous increasing;
- (2) Under the same sand production condition, the liquid-carrying capacity and solid-carrying capacity are significantly enhanced with the increasing volume of foam injection. However, once the foam injection volume is increased to a certain level, the liquid-carrying and solid-carrying effect cannot be significantly improved with the volume of foam injection continuous increasing;
- (3) With the same volume of foam injection, the liquid-carrying capacity and solid-carrying capacity decrease with the increase of water production; the pressure of the bottom hole increases, the temperature of the bottom hole increases; the maximum mixture density increases; the minimum velocity of the gas phase decreases; the minimum velocity of the gas phase decreases and the liquid-carrying capacity decreases, so the minimum velocity of the liquid phase decreases. As the minimum velocity of the gas phase decreases, the solid-carrying capacity decreases, so the minimum velocity of the solid phase decreases; and the minimum gas-holdup ratio decreases. As the minimum gas-holdup rate decreases, the liquid-carrying capacity decreases, so the maximum liquid-holdup rate increases. The minimum gas-holdup rate decreases and the solid-carrying capacity decreases, so the maximum solid phase content increases.
- (4) With the same volume of foam injection, the liquid-carrying capacity and solid-carrying capacity decrease with the increase of sand production; the pressure of the bottom hole increases, the temperature of the bottom hole decreases; the maximum mixture density increases; and the minimum gas phase velocity decreases. As the gas phase velocity decreases, the liquid-carrying capacity decreases, so the minimum velocity of the liquid phase decreases. As the gas phase velocity decreases, the solid-carrying capacity decreases, so the minimum velocity of the solid phase decreases. As the minimum gas-holdup decreases, the maximum liquid-holdup increases, and the maximum solid phase content increases.

Author Contributions: Conceptualization, H.L., N.W. and Z.G.; Methodology, H.L., N.W. and Z.G.; Data curation, H.L.; Validation, F.L., X.W., C.Z., H.X. and J.P.; Formal Analysis, H.L., N.W., Z.G. and B.K.; Resources, L.J. and F.L.; Software, L.J.; Writing—Original Draft Preparation, H.L. and H.H.; Writing-Review & Editing, B.K.; Visualization, F.L., X.W., C.Z., H.X. and J.P.; Investigation, H.H.; Supervision, B.K.; Project Administration, N.W.; Funding Acquisition, N.W. All authors have read and agreed to the published version of the manuscript.

Funding: National Key Research and Development Program (No. 2021YFC2800903), National Natural Science Foundation of China (No. U20B6005-05), 111 Project (No. D21025), Open Fund Project of State Key Laboratory of Oil and Gas Reservoir Geology and Exploitation (No. PLN2021-01, PLN2021-02, PLN2021-03) and Natural Science Foundation of Sichuan Province (No. 2022NSFSC0264, No. 2022NSFSC1088 and No. 2022NSFSC1226).

Data Availability Statement: Not applicable.

Acknowledgments: This research was supported by State Key Laboratory of Oil and Gas Reservoir Geology and Exploitation, State Key Laboratory of Coal Mine Disaster Dynamics and Control, and Chengdu Advanced Metal Material Industrial Technology Research Institute Co., Ltd.

Conflicts of Interest: The authors declare no conflict of interest.

References

1. Fu, Q.; Zhou, S.; Li, Q. Natural Gas Hydrate Exploration and Production Technology Research Status and Development Strategy. *Strateg. Study CAE* **2015**, *9*, 123–132.
2. Kang, J. Experimental Study on Auxiliary Heating Simulation of Natural Gas Hydrate Depressurization Production Well. Master's Thesis, Jilin University, Changchun, China, 2020.
3. Sun, W. Multiphase Nonequilibrium Pipe Flow in Solid Fluidization Exploitation of Marine Natural Gas Hydrate Reservoir. Master's Thesis, Southwest Petroleum University, Chengdu, China, 2016.
4. Xin, G.; Lan, L. *Operation of Industrial Boiler and Operation Practice of Energy Saving and Emission Reduction*; First Machine Press: Beijing, China, 2015; pp. 115–120.
5. Zhao, J.; Li, H.; Zhang, L.; Sun, W.; Wu, K.; Li, Q.; Zhao, J.; Lv, X.; Wang, G. Large-scale physical simulation experiment of solid fluidization exploitation of marine gas hydrate. *Nat. Gas Ind. B* **2018**, *38*, 76–83.
6. Zhou, S.; Chen, W.; Li, Q.; Zhou, J.; Shi, H. Research on the solid fluidization well testing and production for shallow non-diagenetic natural gas hydrate in deep water area. *China Offshore Oil Gas* **2017**, *29*, 1–8.
7. Qiu, Y. Study on Decomposition Law of Marine Non-Diagenetic Natural Gas Hydrate in Solid Fluidization Mining Process. Master's Thesis, Southwest Petroleum University, Chengdu, China, 2016.
8. Peng, Y.; Su, Z.; Liu, L.; Jin, G.; Wei, X. Numerical study on the movement of the decomposition front of gas hydrate depressurization exploitation. *Mar. Geol. Quat. Geol.* **2020**, *40*, 198–207.
9. Hong, R. Study on Factors Affecting Steam Injection of Natural Gas Hydrate. Master's Thesis, Liaoning University of Petrochemical Technology, Fushun, China, 2019.
10. Gao, J. Influence of gas hydrate secondary formation and permeability change on depressurization production. *China Chem. Ind. Trade* **2018**, *19*, 230.
11. Lu, J.; Li, D.; He, Y.; Liang, D.; Xiong, Y. Research status of sand production during natural gas hydrate exploitation. *Prog. New Energy* **2017**, *5*, 394–402.
12. Che, C.; Zhu, Y. New energy in the 21st century: Natural gas hydrate. *Ziguangge* **2014**, *2*, 68–69.
13. Wang, W. Numerical Simulation Research on Gas Hydrate Depressurization Production. Master's Thesis, Qilu University of Technology, Jinan, China, 2021.
14. Sun, H. Research on the Liquid-Carrying Capacity of Gas in Pipelines. Master's Thesis, China University of Petroleum (Beijing), Beijing, China, 2017.
15. Liu, T.; Guo, X.; Wang, S.; Chen, H.; Liu, D. Experimental study on wellbore flow pattern in horizontal well foam drainage and gas production. *Drill. Prod. Technol.* **2017**, *40*, 69–73.
16. Sun, M. Numerical Simulation Research and Application of Foam Fluid Sand Washing and Flushing. Ph.D. Thesis, China University of Petroleum (East China), Qingdao, China, 2007.
17. Xiong, Y.; Jia, J.; Liu, S.; Jiang, Z.; Ren, Y.; Wu, W.; Long, S. Study and Performance Evaluation of Foaming Agent for High Temperature Resistant foam Drainage. *Chem. Eng. Oil Gas* **2012**, *41*, 308–310+359.
18. van Nimwegen, A.T.; Portela, L.M.; Henkes, R.A.W.M. The effect of surfactants on upward air–water pipe flow at various inclinations. *Int. J. Multiph. Flow* **2016**, *78*, 132–147. [[CrossRef](#)]
19. Huang, B.; Nan, X.; Cheng, F.; Zhou, W.; Fu, S.; Zhang, T. Study on foam transport mechanism and influencing factors in foam drainage gas recovery of natural gas well. *J. Dispers. Sci. Technol.* **2022**, *43*, 2049–2057. [[CrossRef](#)]
20. Huang, B.; Nan, X.; Fu, C.; Tang, B.; Wang, S.; Zhang, L.; Guo, W. Investigation on working principle of pipe string for liquid retention and refoaming in the wellbore of natural gas well with foam drainage gas recovery. *Energy Sources Part A Recovery Util. Environ. Eff.* **2021**, *23*, 1–16. [[CrossRef](#)]
21. Chamkha, A.J.; Peddieson, J., Jr. Boundary Layer Theory for a Particulate Suspension. *J. Fluids Eng. Trans. ASME* **1994**, *116*, 147–153. [[CrossRef](#)]
22. Chamkha, A.J. Compressible Two-Phase Boundary-Layer Flow with Finite Particulate Volume Fraction. *Int. J. Eng. Sci.* **1996**, *34*, 1409–1422. [[CrossRef](#)]
23. Chamkha, A.J. Particulate Viscous Effects on the Compressible Boundary-Layer Two-Phase Flow Over a Flat Plate. *Int. Commun. Heat Mass Transf.* **1998**, *25*, 279–288. [[CrossRef](#)]
24. Chamkha, A.J. Effect of Combined Particle-Phase Diffusivity and Viscosity on the Compressible Boundary Layer of a Particulate Suspension over a Flat Surface. *J. Heat Transf.* **1999**, *121*, 420–429. [[CrossRef](#)]
25. Derikvand, Z.; Riazi, M. Experimental investigation of a novel foam formulation to improve foam quality. *J. Mol. Liq.* **2016**, *224*, 1311–1318. [[CrossRef](#)]

26. Du, Z.; Shi, L.; Yang, X.; Zhang, W.; Zhou, H.; Zhao, W.; Wang, G. The research and application of coiled tubing technology of horizontal well in drainage gas recovery. In Proceedings of the International Conference of Green Buildings and Environmental Management (GBEM), Qingdao, China, 23–25 August 2018.
27. Li, R.; Chen, X.; Chang, Y.; Zhang, L.; Zhang, Y.; Zhu, Y.; Wang, T. Increase of bubble size playing a critical role in foam-induced protein aggregation: Aggregation of BSA in foam fractionation. *Chem. Eng. Sci.* **2018**, *174*, 387–395. [[CrossRef](#)]
28. Wen, Y.; Lai, N.; Li, W.; Zhang, Y.; Du, Z.; Han, L.; Song, Z. Factors influencing the stability of natural gas foam prepared by alkyl polyglycosides and its decay rules. *J. Pet. Sci. Eng.* **2021**, *196*, 108039. [[CrossRef](#)]
29. Wang, H.; Liu, J.; Yang, Q.; Wang, Y.; Li, S.; Sun, S.; Hu, S. Study on the influence of the external conditions and internal components on foam performance in gas recovery. *Chem. Eng. Sci.* **2021**, *231*, 116279. [[CrossRef](#)]
30. Fan, X.; Guan, X.; Zhang, M.; Liu, Y.; Li, Y. Aqueous foam synergistically stabilized by the composite of lignin nanoparticles and surfactant. *Colloids Surf. A Physicochem. Eng. Asp.* **2022**, *643*, 128727. [[CrossRef](#)]
31. Lai, N.; Zhang, C.; Wang, J.; Tang, L.; Ye, Z. Effects of Different Gases on the Molecular Behavior of Alkyl Glycosides at Gas/Liquid Interface and Foam Stability. *ChemistrySelect* **2023**, *7*, e202203090. [[CrossRef](#)]
32. Li, S. Research on Foam Sand Washing Technology for Horizontal Wells. Master's Thesis, China University of Petroleum (East China), Qingdao, China, 2006.
33. Ramey, H.J. Wellbore heat transmission. *J. Pet. Technol.* **1962**, *14*, 427–435. [[CrossRef](#)]

Disclaimer/Publisher's Note: The statements, opinions and data contained in all publications are solely those of the individual author(s) and contributor(s) and not of MDPI and/or the editor(s). MDPI and/or the editor(s) disclaim responsibility for any injury to people or property resulting from any ideas, methods, instructions or products referred to in the content.